Toward Transparent Nanocomposites Based on Polystyrene Matrix and PMMA-Grafted CeO$_2$ Nanoparticles

Onur Parlak[†] and Mustafa M. Demir*,[‡]

[†]Department of Chemistry, and [‡]Materials Science and Engineering Program, İzmir Institute of Technology, Gülbahçe Köyü, Urla 35430 İzmir, Turkey

S Supporting Information

ABSTRACT: The association of transparent polymer and nanosized pigment particles offers attractive optical materials for various potential and existing applications. However, the particles embedded into polymers scatter light due to refractive index (RI) mismatch and reduce transparency of the resulting composite material. In this study, optical composites based on polystyrene (PS) matrix and poly(methyl methacrylate) (PMMA)-grafted CeO$_2$ hybrid particles were prepared. CeO$_2$ nanoparticles with an average diameter of 18 ± 8 nm were precipitated by treating Ce(NO$_3$)$\cdot$6H$_2$O with urea in the presence of a polymerizable surfactant, 3-methacyloxypropyltrimethoxy silane. PMMA chains were grafted on the surface of the nanoparticles upon free radical in situ solution polymerization. While blending of unmodified CeO$_2$ particles with PS resulted in opaque films, the transparency of the composite films was remarkably enhanced when prepared by PMMA-grafted CeO$_2$ hybrid particles, particularly those having a PMMA thickness of 9 nm. The improvement in transparency is presumably due to the reduction in RI mismatch between CeO$_2$ particles and the PS matrix when using PMMA chains at the interface.

Invisible particles !

CeO$_2$@PMMA / PS

$n_{Ceria} > n_{PS} > n_{PMMA}$

KEYWORDS: ceria, core–shell nanoparticle, light scattering, index matching, polymerizable surfactant, optical nanocomposites
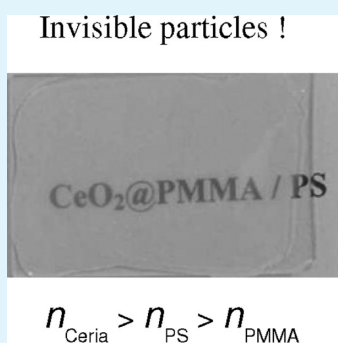
■ INTRODUCTION

Optical materials have attracted considerable attention in recent years due to advances in information and telecommunication technologies. They play key roles in optical assemblies like optical waveguides in communication methods of all kinds,[1−3] display coatings in monitors of electronic devices,[4] and lenses where the ability to control focusing power is required.[5] Because they are optically clear materials, inorganic glasses have been commonly used for these applications. However, the high processing cost and low impact resistance of inorganic glass has driven the development of low-cost, flexible, optically clear materials. One approach is to combine a transparent polymer with nanosized nanosized pigment particles; this not only results in materials with better impact resistance but also results in the polymer having absorption/emission in the desired region of the optical spectrum, high/low refractive indices, and nonlinear optical properties.[6−9] Following this approach, material scientists have sought to develop novel composites using many polymer/nanoparticle composite systems.[10−15] Some examples are ZnO/PMMA,[16,17] ZnO/poly(hydroxyethyl methacrylate),[18] Al$_2$O$_3$/polycarbonate,[19] TiO$_2$/poly(vinyl alcohol),[20] CdS/PS,[10] CdS/PMMA,[21] ZrO$_2$/PMMA,[22] CdTe/PS,[23] and BaTiO$_3$/polyimide.[24] However, the refractive indices (RIs) of polymers and inorganic particles are usually different. Inorganic pigment particles, in general, have an RI in between 2.0 and 3.5; on the other hand, the RI of polymers lies in the range of 1.5−2.0.[25] A sharp refractive index increase at the interface of pigment particles and the surrounding polymer matrix results in strong scattering and as

a result, the optical clarity of composite systems can rapidly diminish.[26] Rayleigh scattering has been used to explained these systems, assuming that the particles are small, dielectric (nonabsorbing), and spherical. Intensity loss originating from this type of scattering can be estimated from the following formula[27]

$$ T = \exp\left[-\frac{3\phi r^3}{4\lambda^4}\left(\frac{n_p}{n_m} - 1\right) \right] s \tag{1} $$

where T is the transmission, s is the optical path length (thickness of the film), r is the radius of the scatterer, ϕ is the volume fraction of particles, n_p and n_m are the refractive indices of the particles and the polymer matrix, respectively, and λ is the wavelength of the incident light. Scatterers in the composite systems refer to particle domains that are either one individual particle or aggregates/agglomerates of the individual particles. A slight increase in the size of the domains causes a dramatic increase in scattering intensity. Considering the strong tendency of nanosized particles to form large aggregates/agglomerates, the development of transparency in polymer nanocomposites is demanding from a synthetic point of view. Therefore, intensive work has focused on nonaggregated particles in a polymer matrix through sophisticated control over the size of both individual

particle and particle domains in a polymer matrix. However, we previously demonstrated that even if the particles are in range of 20—40 nm and nonaggregated, the scattering cannot be completely prevented and the achievement of optical clarity for polymer/particle nanocomposites still remains a challenge.[28,29] In fact, the light scattering originates from discontinuities in refractive index within the internal structure of materials.[26] Following eq 1, when perfect RI matching between particle and polymer is provided (meaning that n_p/n_m goes to 1), T asymptotically approaches 1 (i.e., complete transparency is eventually achieved). Therefore, RI matching becomes a promising approach to improve transparency of composite systems.

The choice of inorganic pigment particles, whose RI is close to that of the surrounding transparent polymer matrix, mediates the transparency of polymer nanocomposites. $SiO_2/PMMA$[30] and CeF_3/PS[31] are prominent examples from the recent literature where transparency is maintained even at high particle contents. However, the toolbox of commercial materials to design RI matching is limited for both transparent polymers and pigment particles. Recent progress in the fabrication of well-defined binary mixtures of inorganics[32,33] and nanostructures[34,35] has allowed the development of transparent polymer nanocomposites. In the former, the solid solution of light and heavy metal oxides (for example Ta_2O_5/SiO_2) is combined in the structure of particles. In the latter, core—shell type nanostructured particles are used. The inorganic core is covered by a shell whose RI is lower than the indices of both core particle and polymer matrix such that the indices of the entire core—shell system is lowered to that of the RI of the polymer matrix, ($n_{core} > n_{shell} > n_{matrix}$). Thus, light cannot differentiate whether the particle domains are scatterers and the composite material readily transmits light. Recently, Li et al. reported the synthesis of highly transparent polymer nanocomposites by incorporation of nanostructured core—shell type silica—titania nanoparticles in the epoxy matrix.[35] The transmittance of the particle loaded epoxy composites was investigated as a function of mass composition $m(TiO_2)/m(SiO_2)$ ranging from 0 to 60 wt %. It was claimed that the optimal transmittance of the nanocomposite was attained at a TiO_2 shell content of 36.5 wt % when RI matching is satisfied.[35]

In the present work, a ternary composite of $PS/CeO_2/PMMA$ was used as a model system to examine the index matching approach. Well-defined CeO_2 (ceria) core and PMMA shell particles were prepared using a robust and simple pathway, and these nanostructured particles were embedded into a transparent PS matrix. Ceria is a yellow pigment and wide band gap semiconductor that has been used as a UV blocking agent.[36] PS is a colorless thermoplastic polymer used in various fields such as packing material, plastic models, insulation materials.[37] It presents high chemical stability, good mechanical properties, and transparency (atactic PS). The association of PS with CeO_2 particles is a reasonable combination for optical applications mentioned above.[38—40] However, there is a strong RI mismatch between PS and CeO_2 particles; direct blending of PS and unmodified CeO_2 particles yields opaque composites. The respective refractive indices of n_{CeO_2}[41] and n_{PS}[42] are 2.20 and 1.59 at 633 nm. The mismatch in refractive indice between PS matrix and CeO_2 can be offset by a third component, whose index is lower than that of both CeO_2 and PS. PMMA is a candidate for this purpose as it has a RI of 1.49 at 633 nm.[42] Because $n_{CeO_2} > n_{PS} > n_{PMMA}$, materials fulfilled the index matching condition when the appropriate composition of

CeO_2 and PMMA are used. It was demonstrated that CeO_2 particles contribute less scattering when they are coated with PMMA chains of a particular layer thickness.

■ EXPERIMENTAL SECTION

Materials. Cerium nitrate hexahydrate $(Ce(NO_3)_3 \cdot 6H_2O)$ (99.9%) was obtained from Fluka. Urea $(CO(NH_2))$ (ACS reagent, 99.0%), 3-Methacryloxypropyltrimethoxysilane (MPS) (99.0%), tetrahydrofuran (THF) (99.9%), and polystyrene (PS) were purchased from Sigma Aldrich and they were used without further purification. Dimethyl formamide (DMF) (99.0%) and toluene (99.5%) were obtained from Riedel de Häen, and were used as received. Methyl methacrylate (MMA) (Fluka, stabilized with 10—20 ppm hydroquinone monometyl ether) was distilled under reduced pressure. Benzoyl peroxide (BPO) was provided from Fluka and recrystallized from methanol.

Precipitation of MPS-Modified CeO_2 Nanoparticles. Nanosized ceria (CeO_2) particles were precipitated from a solution of $(Ce(NO_3)_3 \cdot 6H_2O)$ and urea in DMF. In a typical synthesis, 12.5 mL of 1.5 M urea solution was dropped at a rate of 2—3 mL min^{-1} from a syringe into an equal volume of 0.5 M $Ce(NO_3)_3 \cdot 6H_2O$ solution at 120 °C, then refluxed under mild stirring. At the beginning of the reaction, the mixture was clear. After 15 min of reaction, it turned translucent indicating that nucleation of CeO_2 particles had started. After 1 h reaction time, the mixture turned into an opaque dispersion. For surface modification of nanosized CeO_2 particles, 0.5 mL of MPS in 5 mL of DMF was injected dropwise to the above suspension under nitrogen atmosphere. The reactor was quenched to 0—10 °C right before the addition of the surfactant to prevent self-polymerization of MPS at high temperature. This in situ surface modification was carried out for 12 h more to achieve a uniform surface coverage. The resulting suspensions were subjected to three cycles of centrifugation to isolate the MPS-modified CeO_2 nanoparticles. The particles were washed with fresh ethanol to remove excess MPS and were dried in a vacuum at 50 °C for 8 h prior to in situ polymerization.

Preparation of PMMA-Grafted CeO_2 Hybrid Particles. The MPS-modified CeO_2 particles (20.0 mg) were dispersed in a mixture of MMA-toluene (10:20 in mL). The polymerization was carried out in the presence of these particles at 60 °C using BPO as an initiator at different concentrations (0.5, 1.0, 1.5, and 2.0, 4.0, 6.0 wt %). The particle content was fixed to 0.1 wt % with respect to the amount of MMA. The dispersions in MMA-toluene mixture were sonicated for 15 min and kept overnight in the dispersed state to provide complete wetting of particle surfaces. After a second sonication for 15 min, BPO was added the dispersion. Three cycles of a freeze—thaw process were applied to the dispersions prior to polymerization. The flask containing MPS-modified ceria particles and MMA/toluene mixture were placed into a preheated oil-bath at 60 °C. The polymerization proceeded under nitrogen atmosphere for 6 h, and it was then quenched to room temperature. The resulting hybrid particles (CeO_2 core—PMMA shell) were isolated by three cycles of centrifugation and washing with THF to remove unreacted monomer and free polymers in the polymerization mixture. The hybrid particles were then dried under vacuum at 40 °C for 12 h.

Preparation of PS/PMMA-Grafted CeO_2 Nanocomposite Films. The CeO_2 core-PMMA shell particles were dispersed in a solution PS-THF (20.0 wt % PS), and kept overnight in the dispersed state by stirring. For each dispersion, CeO_2 content was kept constant at 5.0 wt % (0.8 vol %). After sonication for 30 min, composite films were prepared using a Model WS 400B Spin Coater (Laurell Technologies Corp.,North Wales) on glass or quartz substrates.

Characterization. X-ray diffractograms were obtained from a Philips X'pert Pro X-ray Diffractometer using Cu Kα radiation (λ = 1.5418 Å). The size of particles was determined by using a Nano ZS dynamic light scattering instrument (Malvern, Worcestershire).

Scheme 1. Schematic Diagram for the Preparation of Optical PS Composite Films Prepared by PMMA-Grafted CeO₂ Hybrid Particles
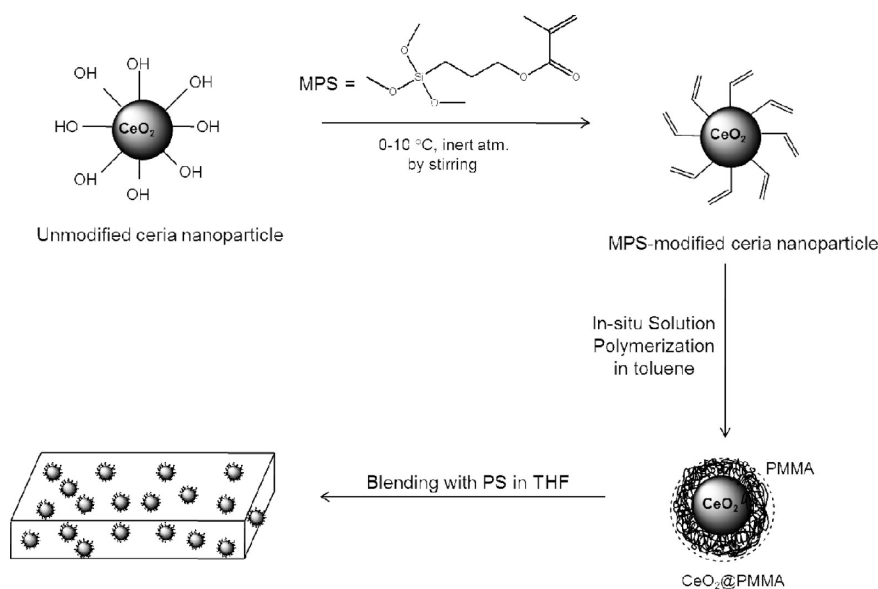
Thermogravimetric analysis was carried out using a Diamond TG/DTA (Perkin-Elmer, Massachusettes). An atomic force microscope, Nanoscope IV (Digital Instruments-MMSPM, New York) was used to investigate the dispersion of the particles in PS matrix. The size distributions of MPS-coated (no PMMA grafting) and PMMA-grafted CeO₂ in PS matrix were obtained from statistical treatment of AFM images by measuring the diameter of typically not less than 50 particles with the help of the software Nanoscope (Veeco, Plainview). Transmission of the nanocomposites was measured with a Cary 50 UV–vis Spectrometer (Varian, Palo Alto). Transmission electron microscopy (TEM) was performed using a G² Spirit/Biotwin (FEI-Technai, Oregon), with a working voltage of 120 kV. FTIR measurements were carried out using PE 100 FTIR spectrometer (Perkin-Elmer, Massachusetts). Film thicknesses were measured with a profilometer using a Dektak 150 (Veeco, Plainview).

■ RESULTS AND DISCUSSION

Scheme 1 outlines the entire process for the preparation of PS/CeO₂/PMMA composites. The synthesis strategy is, first, to form core–shell type nanostructured hybrid particles with a controlled shell thickness. This is the key step to control transparency of the composite material. The second step involves solution blending of these particles with a transparent polymer. The polymer/particle dispersion in THF is then cast on a substrate to obtain an optical composite film.

Preparation of PMMA-Grafted CeO₂ Nanoparticles. Nanosized CeO₂ particles were prepared by precipitation of Ce-(NO₃)₃·6H₂O and urea in DMF at 120 °C for 1 h. Figure S1 in the Supporting Information shows powder the X-ray diffraction (XRD) pattern of unmodified CeO₂ nanoparticles. As seen, the characteristic reflections of cubic flourite structure (JCPDS-34–0394) CeO₂ are present. Using Debye–Scherrer line broadening, we found the size of the crystallite particles to be 16 nm.

A polymerizable surfactant (3-methaxcryloxypropyl trimethoxysilane) (MPS) was added into reaction mixture during the particle nucleation and growth process. CeO₂ particles, like all oxidic ones, are inevitably covered by surface hydroxyl groups.[28] A hydrolysis reaction takes place between surface OH and silanol groups of MPS such that MPS is immobilized to the particle surface through chemical bonding and the vinyl groups of the molecules remain free on the surface of particles. MPS, in this system, has three functions: (i) MPS molecules grafted to the particles hinder the diffusion of reactants to/from the surface, i.e., it controls the growth of the nanoparticles; (ii) stabilization of the particle dispersion and redispersibility in an organic medium; (iii) MPS provides an anchor for the generation of polymer shell layers due to the presence of the available vinyl groups.

The MPS-modified particles were dispersed into an equivolume mixture of MMA-toluene and polymerization was carried out in situ by a free radical initiator (BPO). The vinyl groups on the particles' surface are reactive and contribute to the polymerization of MMA. Eventually, the particles are covered with a PMMA layer. It must be noted that to obtain well-defined PMMA-grafted CeO₂ particles, the particle content must be carefully adjusted because it determines interparticle distance in the process of in situ polymerization. If a polymer chain appears to be longer than the average interparticle distance, it may interact with more than one particle; and each particle in the medium is linked by many chains. Such being the case, a three-dimensional network where CeO₂ nanoparticles are placed at the junction points is developed throughout the reactor volume and the particles cannot be isolated from the system by dissolution. Thus, the particle content in the in situ polymerization should be kept low (~0.1 wt %) to prevent the formation of an undesirable network structure.

Figure 1 presents the number size distribution of MPS-modified and PMMA-grafted CeO₂ hybrid particles prepared at different BPO concentrations. The results were obtained by DLS in toluene. Although MPS-modified CeO₂ particles exhibit uniform size distribution with a mean diameter of 18 nm, the size of PMMA-grafted CeO₂ hybrid particles extends to large diameters depending on the amount of BPO employed. The diameter of the hybrid particles was found to be inversely proportional to BPO concentration. For example, the mean diameter of the hybrid particles was 36 nm when the amount of BPO was 6 wt %. As BPO content was reduced to 0.5 wt %, the mean of the particle size distribution increased gradually to
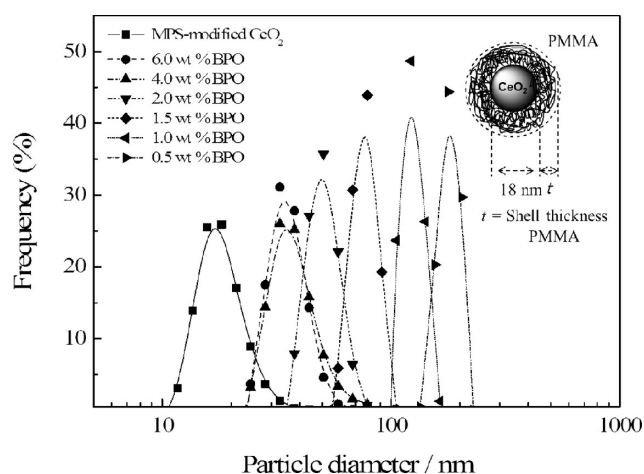
Figure 1. DLS number size distribution of CeO_2 core and PMMA-grafted CeO_2 particles at varying shell thickness in toluene.
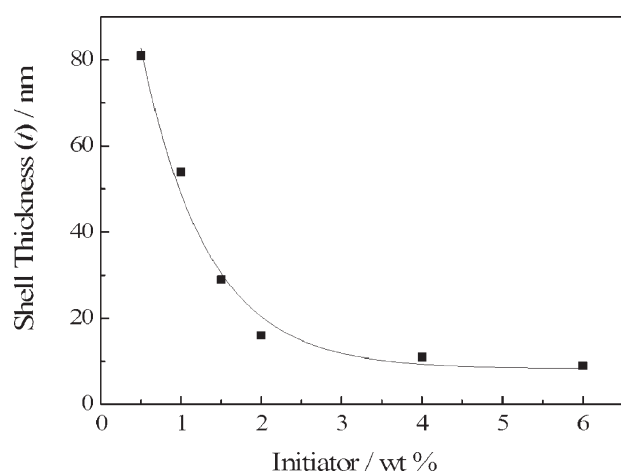

Figure 2. Thickness of PMMA shell on CeO_2 core particle as a function of initiator (BPO) content.

186 nm. PMMA-grafted CeO_2 hybrid particles have a core–shell nanostructure. The diameter of the CeO_2 core was fixed at 18 nm and the PMMA shell varied depending on the initiator content employed during polymerization. Assuming that the core particles have a spherical shape and because of the uniform grafting of PMMA chains on the particles, the PMMA shell thickness (t) can be obtained by subtracting the diameter of the CeO_2 core from the mean diameter of PMMA-grafted CeO_2 particles. Figure 2 shows the thickness of the PMMA layer estimated by this subtraction as a function of BPO content. The thickness showed a first-order decay as the initiator concentration was increased.

To make a rough estimation about the size of the average PMMA chain, polymerization was carried out in the absence of the hybrid particles using the same conditions (temperature, time, solvent, and initiator content) that had been employed in the process of in situ polymerization. On the basis of this experiment, the thickness of the PMMA layer was found to be greater than the size of an average chain. For example, the diameter of the PMMA coil was 10 nm when the BPO concentration was 1.5 wt %. In comparison, at the same BPO content in the presence of the hybrid particles, the thickness of the shell was 29 nm. This result indicates the existence of the multilayer
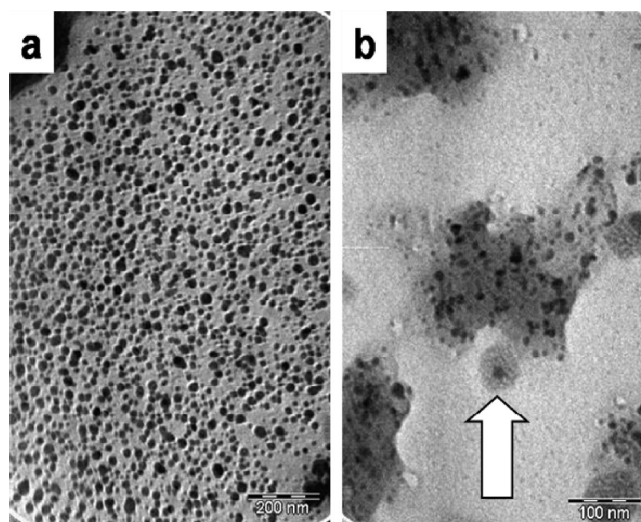

Figure 3. TEM images obtained from (a) as-synthesized CeO_2 and (b) representative PMMA-grafted CeO_2 hybrid particles with 16 nm PMMA thickness.

grafting of PMMA chains on the surface of the CeO_2 core. In the first layer, PMMA chains are chemically linked at one or more sites to the surface of the particles through MPS. In the second layer, the chains are physically adsorbed to the first layer. The adsorption occurs several times layer-by-layer radially outward from the surface of the particles. This process eventually forms a PMMA layer around each particle. This layer makes the hybrid particles sterically stabilized against aggregation and sedimentation such that the same particle size distribution was even obtained from the hybrid particles after 1 week. The long-term stability of the particles demonstrates that any detachment of the chains from the particle surface does not occur, at least within the time period investigated.

A drop of PMMA-grafted CeO_2 particle dispersion from toluene was cast on a TEM grid. After evaporation of the solvent, the surface was examined by TEM. Figure 3 shows TEM images of MPS-modified and PMMA-grafted CeO_2 particles. Panel a shows an overview image of MPS-modified CeO_2 particles in a well-dispersed state. The particles are spherical and have uniform size. An average particle diameter of 18 ± 8 nm was measured from 100 particles, which is consistent with the size measured by DLS ($d = 18$ nm). While the MPS-modified CeO_2 particles were well separated on the carbon film of the TEM grid, the PMMA-grafted CeO_2 particles appeared in islands of particle domains (Panel b). Obtaining an image of an individual colloidal particle is a difficult task because solvent evaporation from the droplet used for TEM imaging invariably causes the formation of phase-separated particle domains. The core CeO_2 particles are evident in the clusters. Nevertheless, the white arrow in the image shows a representative individual PMMA-grafted CeO_2 particle. This hybrid particle can be considered to be an indication of the formation of a core–shell type nanostructure.

To measure the relative mass of the inorganic core to the organic shell in the particle system, we evaluated unmodified CeO_2, MPS-modified CeO_2, and PMMA-grafted CeO_2 particles with varying PMMA thicknesses using TGA (Figure 4). For the unmodified and MPS modified particles, mass loss of nearly 4 wt % takes place below 300 °C because of the loss of adsorbed water. However, MPS-modified particles have nearly 2.5 wt % higher
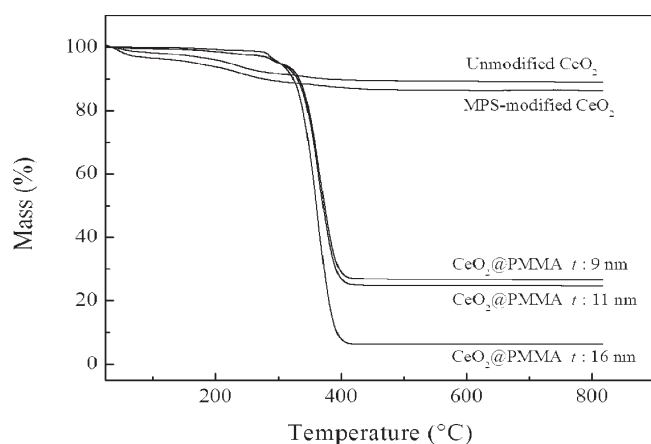
Figure 4. TGA curves for unmodified, MPS-modified, and PMMA-grafted CeO$_2$ particles.
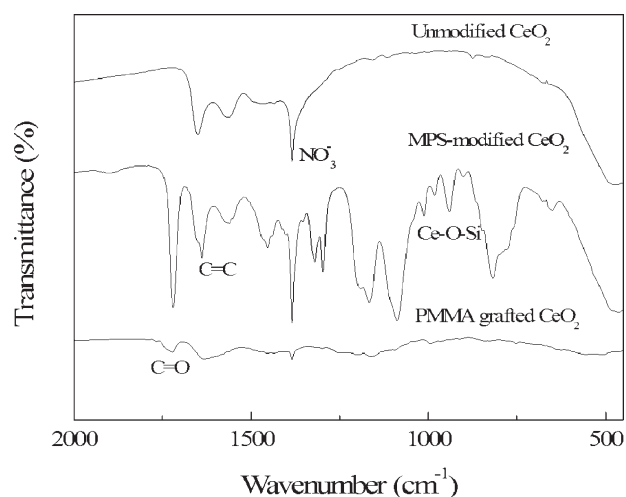

Figure 5. FTIR spectra of unmodified, MPS-modified, and PMMA-grafted CeO$_2$ particles.

mass loss compared to unmodified ones. This difference can be attributed to dehydration of silane groups on the particle surface. By knowing the mass loss of MPS and the particle size from DLS, the graft density of MPS on the particles can be estimated assuming monolayer coverage on the spherical CeO$_2$ particles. On the basis of this calculation, the graft density of MPS molecules was found to be 1.4 molecules/nm^2. In the thermogram of PMMA-grafted particles, a sharp mass loss was observed between 300 and 400 °C because of the thermal oxidation and decomposition of the PMMA layer grafted onto the CeO$_2$ particles. As a result of the disappearance of polymeric residue, the mass remains almost unchanged above 400 °C. This refers to an inorganic residue mainly composed of CeO$_2$. The mass loss beyond this temperature gives clues about the amount of PMMA layer on the ceria particles. Considering that the size of the CeO$_2$ core is fixed and only shell thickness varies, the PMMA-grafted CeO$_2$ particles having a greater shell thickness are undergoing higher mass loss. The amount of PMMA was found to be 73, 75, and 93 wt % for particles having shell thicknesses of 9, 11, and 16 nm, respectively.

The modification of the CeO$_2$ nanoparticles by MPS and grafting with PMMA was validated by vibrational spectroscopy. The FTIR spectra of unmodified CeO$_2$, MPS-modified CeO$_2$,
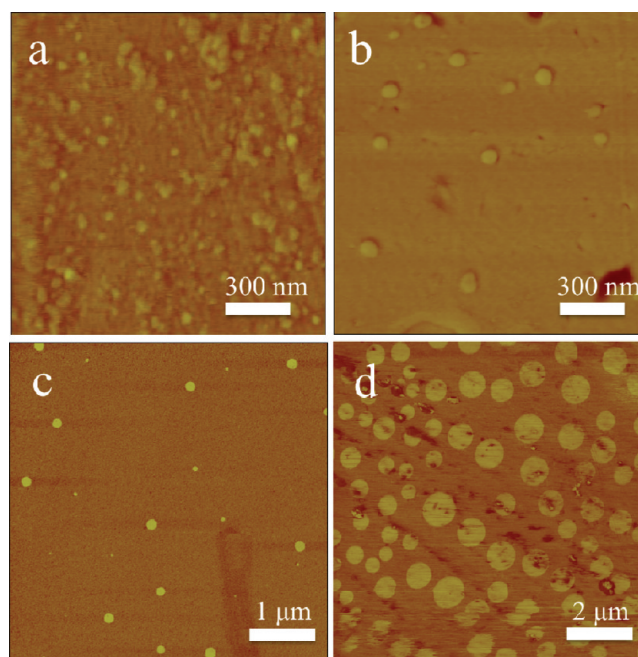

Figure 6. Tapping mode AFM phase images of PS composites loaded with (a) MPS-capped CeO$_2$ particles, (b) PMMA-grafted CeO$_2$ particles having a PMMA thickness of 9 nm, (c) PMMA-grafted CeO$_2$ particles having a PMMA thickness of 29 nm, and (d) PS-PMMA blend without CeO$_2$ nanoparticles.

and PMMA-grafted CeO$_2$ nanoparticles are shown in Figure 5. The strong absorption band at 1384 cm^{-1} is present in all three spectra regardless of the surface chemistry of the CeO$_2$ core. This band is attributed to the stretching of NO$_3^-$ groups remaining on the surface of the core CeO$_2$ particles.[43] Upon surface treatment of the particles with MPS, three major signals at 1722, 1638, and 1193−1168 cm^{-1} appear in the spectrum as a result of C=O stretching, C=C stretching, and ester vibration (C−O−C), respectively. This spectrum was compared with the one of MPS itself (see Figure S2 in the Supporting Information). We observed that the signals of adsorbed groups are remarkably broader for surface bound MPS compared to unbound MPS. Moreover, unique bands seen for the case of bound MPS are present in the range of 800−1000 cm^{-1}. They apparently originated from the Ce−O−Si bond, indicating the hydrolysis of the OH groups of the CeO$_2$ surface and silanol groups of MPS. After polymerization of MMA and MPS on the particle surface, the fingerprint signals of the carbonyl group at 1722 and 1600 cm^{-1} are evident in the spectrum.

Preparation of PS/PMMA-Grafted CeO$_2$ Composite Films. A series of optical composites was prepared by blending a solution of PS/THF (20.0 wt % PS) separately with (a) unmodified CeO$_2$ and (b) MPS-modified CeO$_2$. Likewise, separate solutions of PS/THF (20.0 wt % PS) were prepared with PMMA-grafted CeO$_2$ particles, each dispersion containing a different thickness of PMMA. The composite films were examined by AFM to examine the dispersion of PMMA-grafted CeO$_2$ particles in the PS matrix. Panels a, b, and c in Figure 6 show the AFM tapping mode phase images of a PS matrix loaded with MPS-modified CeO$_2$ particles, PMMA-grafted CeO$_2$ particles having thickness of 9 and 29 nm, respectively. The bright regions in the images refer to PMMA immobilized to the CeO$_2$ core. The interaction of the AFM tip is limited to the uppermost layer of a

Table 1. Mean Diameter and Polydispersity Index (PDI) of Particle Size Distribution (PSD) of PMMA-Grafted CeO_2 Hybrid Particles and Average Diameter of the Particle Domains Prepared at Different BPO Concentrations

BPO[a]	DLS size (nm)[b]	PDI of PSD[c]	AFM size (nm)[d]
6.0	36	0.4	30 ± 6
4.0	40	0.4	45 ± 15
1.5	76	0.4	57 ± 19
1.0	126	0.3	134 ± 100
0.5	187	0.3	236 ± 60.0

[a] PMMA-grafted CeO_2 particles prepared at different BPO concentrations (wt %). [b] Mean of PSD of PMMA-grafted CeO_2 particles determined using DLS in toluene (nm). [c] Polydispersity index of particle size distribution; [d] Average diameter of PMMA-grafted CeO_2 particle domains obtained by AFM in PS (nm).
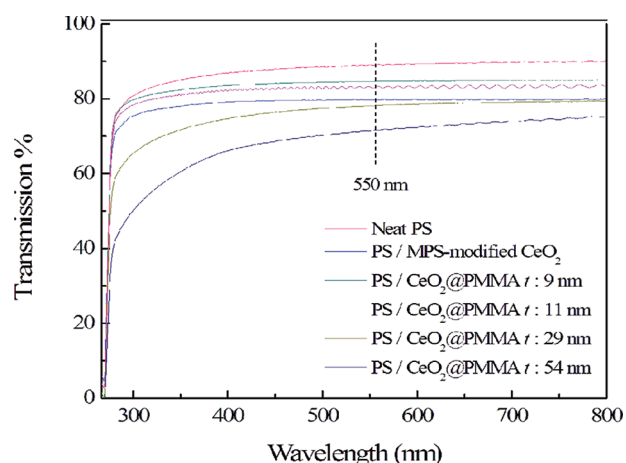

Figure 7. UV−vis transmission spectra of the spin-coated PS composite films prepared by MPS-modified particles and PMMA-grafted CeO_2 particles at varying shell thicknesses. The thickness of the films was around 2.5 μm. The amount of CeO_2 core was fixed to 5.0 wt.% (0.8 vol %).

Figure 8. Transmission values of the all films as a function of PMMA shell thickness at 550 nm. The data points were obtained from the transmission spectra of the films given in Figure 7.

specimen; therefore, the tip mainly encounters PMMA such that the CeO_2 core cannot be resolved from the images. For the purpose of comparison, PS and PMMA chains were blended in the absence of CeO_2 particles. The amount of PMMA in the blend was adjusted to be the same amount as had been employed in the PMMA-grafted CeO_2 particles where t was 9 nm. Not surprisingly, a strong phase separation was observed in the blend film. The results of the tapping mode AFM phase imaging (Panel d of Figure 6) showed that PMMA were dispersed into the PS matrix as spherical domains with a diameter ∼0.5 μm. Phase separation is an equilibrium phenomenon where the chains diffuse to form polymer domains. In our system, a microphase separation does not take place because the chains are immobilized at the nanoparticle surface and diffusion of the chains is hindered.

The average diameter of the PMMA-grafted CeO_2 particles observed by AFM was compared with the mean diameter of particles measured by DLS. The results are given in Table 1. Although the measurement systems are different, the dimensions obtained by these methods approximately agree, particularly at high BPO concentrations. For example, in Panel b, the diameter of particles was found to be 30 ± 6 nm as measured from at least 50 test particles, while the mean diameter of particles was measured as 36 nm by DLS. In contrast, a deviation is observed in the
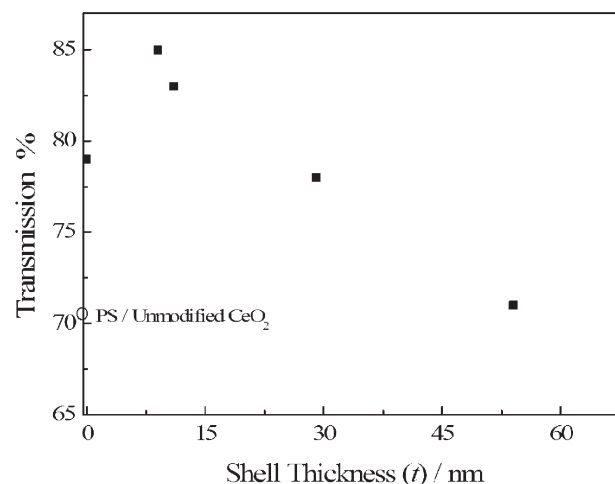
measurements at low BPO concentrations. The decrease in BPO concentration led to the development of longer chains with broader molecular weight distributions via free radical polymerization. The broad distribution of chains reflects the formation of the heterogeneous thickness on the particle surface. Therefore, the distribution obtained by DLS appears broader. In AFM imaging, particles larger/smaller than the mean value are seen in the same micrograph.

Transmission of the Composite Films. The optical composites were spin-coated on quartz glass. The thickness of the resulting films was ∼2.5 μm. Figure 7 shows the UV−vis transmission spectra of both neat PS and PS-based composite films prepared separately using unmodified, MPS-modified, and PMMA-grafted CeO_2 particles. In all composite films, the core CeO_2 content was fixed at 5.0 wt % (0.8 vol %). The films are strongly absorbing in the UV region of the spectrum because both CeO_2 and styrene groups in the PS matrix are absorbing in this region. Ceria is a wide band gap semiconductor whose energy lies between 2.72 and 3.52 eV, depending on the size, shape, and surface chemistry of the particles.[44,45] This energy is comparable to the energy of the UVB region so that it absorbs in this region of the optical spectrum. In addition, styrene involves a benzene group that strongly absorbs UV radiation. The presence of both absorbing entities in the composite material causes a sharp absorption below 300 nm. However, the films are nonabsorbing in the visible region. The intensity loss in this region is mainly due to the scattering from the CeO_2 nanoparticles and PMMA layer. We mainly focus on the visible region where we can compare the intensity loss in PS/ceria composite systems. Since the human eye has the highest sensitivity at 550 nm, the spectra of composites were compared with respect to their transmission at this wavelength. Transmission of all films prepared by PMMA-grafted CeO_2 particles as a function of PMMA shell thickness is given in Figure 8. Neat PS has ∼90% transmission at normal incidence. The loss in this sample occurs due to the reflection of the incident beam from the glass surface and optical scattering from density fluctuations within the internal structure of the PS film. The incorporation of unmodified particles into the PS matrix causes more than a 20% loss in transmission (70%). The unmodified particles were dispersed in the polymer matrix as
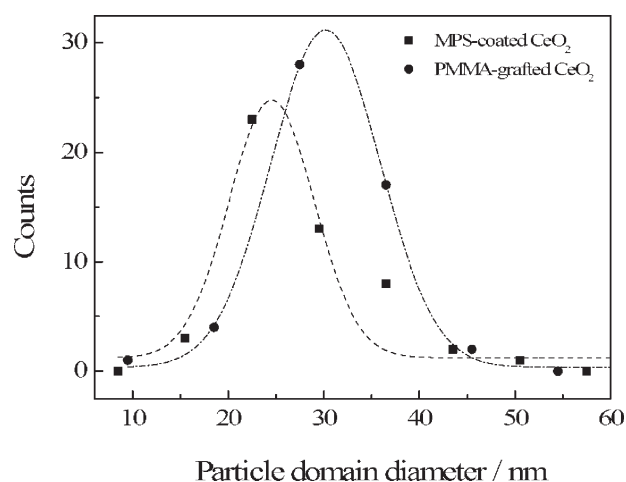
Figure 9. Diameter distributions of MPS-capped CeO_2 particles (a) and PMMA-grafted CeO_2 particle domains with PMMA shell thickness of 9 nm. (b) in PS matrix.

large domains, and the scattering of these domains reduced the transmission of light. The modification of the particle surface with MPS improved dispersion of the particles into smaller domains. Accordingly, this structure causes a 7% increase in transmission (77%). When PMMA-grafted hybrid CeO_2 particles were used with 9 nm of PMMA shell, transmission increased up to a value of 85%. This is the highest value we ever achieved in our study for spin-coated films. As PMMA shell thickness was increased to 29 nm, the transmission through the composite film decreased to 76%. Further increase in thickness of the PMMA shell resulted in a dramatic loss of transparency of the composites. As a result, the transmission of PS nanocomposites prepared by PMMA-grafted CeO_2 particles strongly depends on the thickness of the PMMA shell. The decrease in transparency of composite films prepared by the hybrid particles with greater PMMA thickness very likely arises from scattering of PMMA chains. As the thickness of PMMA was increased, the contribution of PMMA with respect to CeO_2 increased. It would seem that PMMA chains and the CeO_2 core together cause further scattering. To validate this argument, the transmission of the PS and PMMA blend film prepared without CeO_2 particles was measured. Its transmission was found to be 67% at 550 nm, which is the smallest value among all the films. PMMA has a lower RI compared to PS so that the PMMA domains, now, appear to act as a scattering source in the PS matrix and lead to a remarkable decrease in transparency (see Figure S3 in the Supporting Information)

Our main argument in this study is that transmission through the PS/CeO_2 composite system increases when PMMA chains are grafted onto the surface of CeO_2 particles at a particular thickness. Recall that there are two factors that affect intensity loss in heterogeneous composite systems: (i) size of scatterers, and (ii) RI mismatch between the scatters and the surrounding medium. One may argue that the increased transparency in our system may be a result of better particle dispersion, but not because of RI matching. In other words, PMMA chains may act as an efficient surfactant and provide smaller CeO_2 particle domains, giving rise to an analogous decrease in scattering. To clarify this discrepancy, we quantitatively examined size distributions of MPS-coated CeO_2 particles (no PMMA grafting) and PMMA-grafted CeO_2 particles in a PS matrix. Figure 9 shows size distributions
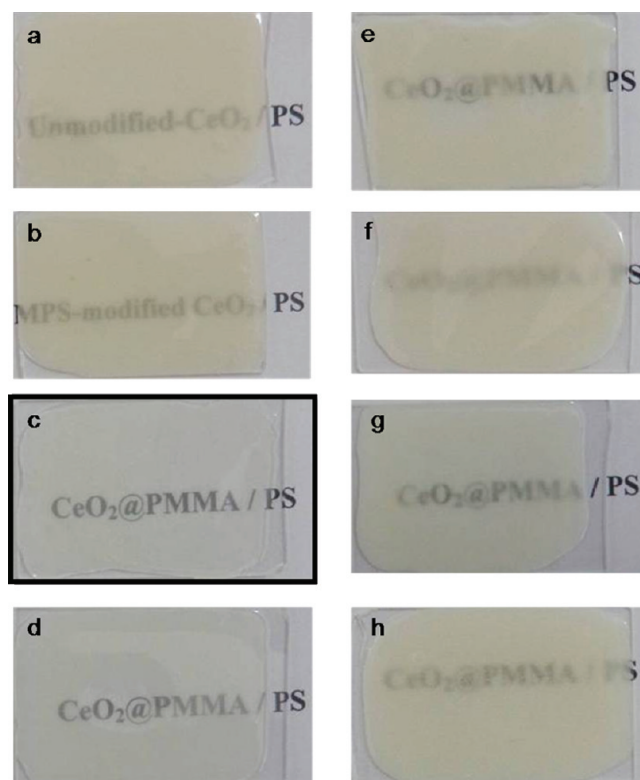

Figure 10. Photographic image of the nanocomposites film prepared by casting. The thickness of the films was around 350 μm. PS composites prepared by (a) unmodified CeO_2 particles (b) MPS modified CeO_2 particles, and PMMA-grafted CeO_2 particles of different PMMA thickness (t). (c) t = 9 nm, (d) t = 11 nm, (e) t = 16 nm, (f) t = 29 nm, (g) t = 54 nm (h) t = 84 nm.

obtained by statistical treatment of the particle domains in AFM images for both systems (Panel a and b of Figure 6). The mean diameter of MPS-coated CeO_2 particle domains was found to be around 21 nm. This size is comparable to the size of an individual particle measured by DLS (Figure 1). For the PMMA-grafted CeO_2 hybrid particles (obtained upon polymerization of MMA in the presence of the MPS-coated CeO_2 particles) where PMMA thickness was 9 nm, the size distribution centered around 29 nm. It can be reasonably claimed that the particles are dispersed individually and nonaggregated in both systems. As a conclusion, the argument based on the increase of transparency due to the size of scatterers, i.e., particle domains, is ruled out.

The index of refraction, n, of a nonmagnetic material is linked to the dielectric constant, ε_r, via the simple relation, $n = \varepsilon_r^{1/2}$.[46] The dielectric constant of core—shell type hybrid particles (ε_{eff}) can be estimated by the Maxwell—Garnett formula

$$\varepsilon_{eff} = \varepsilon_{shell}\left(1 + 3\frac{\phi x}{1 - \phi x}\right) \qquad (2)$$

The variable, x is equal to $1/3\,(\varepsilon_{core} - \varepsilon_{shell})/(\varepsilon_{core} - 1/3\,(\varepsilon_{core} - \varepsilon_{shell}))$, where ϕ is the volume fraction of the CeO_2 core, and $\phi = V_{core}/(V_{core} + V_{shell})$.[47−49] According to this formula, scattering can be diminished if the effective dielectric constant of the core—shell particle is equal to the one of the embedding medium ($\varepsilon_{eff} = \varepsilon_{medium}$). The composition for index matching was estimated for our particular PS/CeO_2 system. See Figure S4 in the Supporting Information presents the estimated RI of overall

core–shell type particles as a function of the thickness of the PMMA shell. For ceria nanoparticles having a diameter of 18 nm, the thickness of CeO_2 particles for index matching should be 7 nm. The thinnest PMMA layer we have obtained in our experiments was 9 nm and the composites prepared when using these particles provided the highest transmission. To adjust the thickness of the PMMA layer to 7 nm to obtain complete matching, we further increased the amount of BPO with the aim of decreasing the layer thickness to 7 nm. However, a PMMA layer thinner than 9 nm was not achieved at all. The search for complete transparency and ex situ preparation of PMMA chains having 7 nm in thickness is underway as a continuation of this study.

The improvement in transmission by index matching is more striking in thicker films and can even be seen by the naked eye. Figure 10 shows the photographic images of the films cast from THF with average thickness of 350 μm. The composite films prepared by (a) unmodified and (b) MPS-modified particles have strong yellowish opacity. An obvious increase in transmission is observed for the composite film containing PMMA-grafted CeO_2 particles which has PMMA shell thickness of 9 nm (c). The increase in the PMMA thickness reduced transmittance and made the composite films opaque (d–h). Thus, the images of all composite films are in congruence with the results obtained via UV–visible transmittance measurements.

CONCLUSION

In this study, we employed a new approach, RI matching, to prepare quasi-transparent polymer/particle composite systems. Core–shell type PMMA-grafted CeO_2 particles were blended with a transparent PS matrix. These hybrid particles were synthesized by combining a precipitated CeO_2 core (prepared under controlled conditions) that has available vinyl groups on its surface that contributes to the free radical in situ solution polymerization of MMA in the presence of these particles. The CeO_2 core of the hybrid particles was fixed at 18 nm in diameter. The thickness of PMMA on the CeO_2 core was readily controlled by the amount of free radical initiator BPO. Blending of PS and neat CeO_2 particles initially resulted in an opaque material. However, its transmittance was remarkably improved when PMMA chains of proper composition were grafted onto the surface of the CeO_2 core. For example, the transmission of spin-coated PS/CeO_2 composite films increased from 71 to 85% when the CeO_2 concentration was 5.0 wt % (0.8 vol %) and when the CeO_2 core was coated with a PMMA layer at a thickness of 9 nm. At this composition, the intensity loss due to optical scattering was remarkably minimized. This approach can be considered as a general strategy for improving optical clarity for various polymer/pigment particle systems.

ASSOCIATED CONTENT

ⓢ Supporting Information. includes XRD pattern of CeO_2 nanoparticles, FTIR of MPS, RI of the PMMA-grafted CeO_2 particles as a function of PMMA thickness, and photographic image of PS/PMMA blend. This material is available free of charge via Internet at http://pubs.acs.org.

AUTHOR INFORMATION

Corresponding Author

*E-mail: mdemir@iyte.edu.tr. Tel.: +90 232 750 75 11. Fax: +90 232 750 75 09.

REFERENCES

(1) Yoshida, M.; Prasad, P. N. *Chem. Mater.* **1996**, *8*, 235–241.
(2) Yamada, N.; Yoshinaga, I.; Katayama, S. *J. Appl. Phys.* **1999**, *85*, 2423–2427.
(3) Chang, C. C.; Chen, W. C. *Chem. Mater.* **2002**, *14*, 4242–4238.
(4) Qi, H.; Hegmann, T. *J. Mater. Chem.* **2008**, *18*, 3288–3294.
(5) Okada, Y.; Murata, A.; Ando, T.; Suenaga, T.; Korenaga, T.; Suzuki, M. *Kobunshi Ronbunshu* **2010**, *67*, 390–396.
(6) Beecroft, L. L.; Ober, C. K. *Chem. Mater.* **1997**, *9*, 1302–1317.
(7) Caseri, W. *Macromol. Rapid Commun.* **2000**, *21*, 705–722.
(8) Lu, C. L.; Yang, B. *J. Mater. Chem.* **2009**, *19*, 2884–2901.
(9) Wegner, G.; Demir, M. M.; Faatz, M.; Gorna, K.; Munoz-Espi, R.; Guillemet, B.; Grohn, F. *Macromol. Res.* **2007**, *15*, 95–99.
(10) Du, H.; Xu, G. Q.; Chin, W. S.; Huang, L.; Ji, W. *Chem. Mater.* **2002**, *14*, 4473–4479.
(11) Kulyk, B.; Sahraoui, B.; Krupka, O.; Kapustianyk, V.; Rudyk, V.; Berdowska, E.; Tkaczyk, S.; Kityk, I. *J. Appl. Phys.* **2009**, *106*, 093102–093102–6.
(12) Asunskis, D. J.; Bolotin, I. L.; Hanley, L. *J. Phys. Chem. C* **2008**, *112*, 9555–9558.
(13) Yuwono, A. H.; Xue, J. M.; Wang, J.; Elim, H. I.; Ji, W. *J. Elect. roceram.* **2006**, *16*, 431–439.
(14) Elim, H. I.; Ji, W.; Yuwono, A. H.; Xue, J. M.; Wang, J. *Appl. Phys. Lett.* **2003**, *82*, 2691–2693.
(15) Feng, M.; Chen, Y.; Gu, L. L.; He, N.; Bai, J. R.; Lin, Y.; Zhan, H. B. *Eur. Poly. J.* **2009**, *45*, 1058–1064.
(16) Demir, M. M.; Memesa, M.; Castignolles, P.; Wegner, G. *Macromol. Rapid Commun.* **2006**, *27*, 763–770.
(17) Hess, S.; Demir, M. M.; Yakutkin, V.; Baluschev, S.; Wegner, G. *Macromol. Rapid Commun.* **2009**, *30*, 394–401.
(18) Hung, C. H.; Whang, W. T. *J. Mater. Chem.* **2005**, *15*, 267–274.
(19) Hakimelahi, H. R.; Hu, L.; Rupp, B. B.; Coleman, M. R. *Polymer* **2010**, *51*, 2494–2502.
(20) Nussbaumer, R. J.; Caseri, W. R.; Smith, P.; Tervoort, T. *Macromol. Mater. Eng.* **2003**, *288*, 44–49.
(21) Khanna, P. K.; Singh, N. *J. Lumin.* **2007**, *127*, 474–482.
(22) Hu, Y. Q.; Zhou, S. X.; Wu, L. M. *Polymer* **2009**, *50*, 3609–3616.
(23) Zhang, H.; Cui, Z. C.; Wang, Y.; Zhang, K.; Ji, X. L.; Lu, C. L.; Yang, B.; Gao, M. Y. *Adv. Mater.* **2003**, *15*, 777–780.
(24) Devaraju, N. G.; Kim, E. S.; Lee, B. I. *Microelectron. Eng.* **2005**, *82*, 71–82.
(25) Caseri, W. *Chem. Eng. Commun.* **2009**, *196*, 549–572.
(26) *Light Scattering by Small Particles*; Hulst, H. C. v. d., Ed.; Dover Publications, New York, 1981; p 91.
(27) Novak, B. M. *Adv. Mater.* **1993**, *5*, 422–433.
(28) Demir, M. M.; Castignolles, P.; Akbey, U.; Wegner, G. *Macromolecules* **2007**, *40*, 4190–4198.
(29) Demir, M. M.; Koynov, K.; Akbey, U.; Bubeck, C.; Park, I.; Lieberwirth, I.; Wegner, G. *Macromolecules* **2007**, *40*, 1089–1100.
(30) Chau, J. L. H.; Hsieh, C. C.; Lin, Y. M.; Li, A. K. *Prog. Org. Coat.* **2008**, *62*, 436–439.
(31) Tan, M. C.; Patil, S. D.; Riman, R. E. *ACS Appl. Mater. Interfaces* **2010**, *2*, 1884–1891.
(32) Schulz, H.; Burtscher, P.; Madler, L. *Composites, Part A* **2007**, *38*, 2451–2459.
(33) Schulz, H.; Madler, L.; Pratsinis, S. E.; Burtscher, P.; Moszner, N. *Adv. Funct. Mater.* **2005**, *15*, 830–837.
(34) Bombalski, L.; Dong, H. C.; Listak, J.; Matyjaszewski, K.; Bockstaller, M. R. *Adv. Mater.* **2007**, *19*, 4486–4490.

(35) Li, Y. Q.; Fu, S. Y.; Yang, Y.; Mai, Y. W. *Chem. Mater.* **2008**, *20*, 2637–2643.

(36) Masui, T.; Fujiwara, K.; Machida, K.; Adachi, G.; Sakata, T.; Mori, H. *Chem. Mater.* **1997**, *9*, 2197–2204.

(37) Rizzo, P.; Alnunia, A. R. *Macromol. Chem. Phys.* **2011**, *212*, 1419–1430.

(38) Taguchi, M.; Takami, S.; Adschiri, T.; Nakane, T.; Sato, K.; Naka, T. *Crystengcomm* **2011**, *13*, 2841–2848.

(39) Dey, A.; Karan, S.; De, S. K. *Solid State Ionics* **2008**, *178*, 1963–1968.

(40) Druffel, T.; Buazza, O.; Lattis, M.; Farmer, S.; Spencer, M.; Mandzy, N.; Grulke, E. A. In *Nanophotonic Materials V*; Gaburro, Z., Cabrini, S., Talapin, D., Eds.; SPIE−International Society for Optical Engineering: Bellingham, WA, 2008; Vol. 7030, p F300.

(41) Zhang, F.; Jin, Q.; Chan, S. W. *J. Appl. Phys.* **2004**, *95*, 4319–4326.

(42) *Polymer Handbook*; 4th ed.; Seferis, J. C., Ed.; Wiley & Sons: New York, 1999, VI, p 571.

(43) Xu, J. X.; Li, L. P.; Li, G. S. *J. Dispersion Sci. Tech.* **2008**, *29*, 1072–1079.

(44) Taguchi, M.; Takami, S.; Naka, T.; Adschiri, T. *Cryst. Growth Des.* **2009**, *9*, 5297–5303.

(45) Chen, H. I.; Chang, H. Y. *Ceram. Int.* **2005**, *31*, 795–802.

(46) Born, M.; Wolf, E. *Principles of Optics*; Cambridge University Press: Cambridge, U.K., 1980; Vol. 7, p 14.

(47) Garnett, J. C. M. *Philos. Trans. R. Soc. London, Ser. A* **1904**, *203*, 385–420.

(48) Garnett, J. C. M. *Philos. Trans. R. Soc. London, Ser. A* **1906**, *205*, 237–288.

(49) Maldovan, M.; Bockstaller, M. R.; Thomas, E. L.; Carter, W. C. *Appl. Phys. B: Lasers Opt.* **2003**, *76*, 877–884.

4314

dx.doi.org/10.1021/am200983h |*ACS Appl. Mater. Interfaces* 2011, 3, 4306–4314